THIRD EUROPEAN ROTORCRAFT AND POWERED LIFT AIRCRAFT FORUM

Paper No. 25

AEROMECHANICAL STABILITY OF SOFT INPLANE HINGELESS ROTOR HELICOPTERS

ROBERT A. ORMISTON

Ames Directorate, Air Mobility R&D Laboratory
U.S. Army Aviation R&D Command
Moffett Field, California

September 7-9, 1977

AIX-EN-PROVENCE, FRANCE

ASSOCIATION AERONAUTIQUE ET ASTRONAUTIQUE DE FRANCE

CORRECTIONS

Paper No. 25

"Aeromechanical Stability of Soft Inplane Hingeless Rotor Helicopters"
by Robert A. Ormiston

Pg. 4 -- The Increase Ω -- Decrease Ω operating line in Fig. 3 should pass through the $\bar{\omega}_\zeta$, $\bar{\omega}_x$ = 0, 0 point rather than 0.1, 0.

Pg. 5 -- The element in the last row, last column of the mass matrix of Eq. (3) should be $2I_\theta/bI$ rather than 1.

Pg. 6 -- Third line, second paragraph, the word "pylon" should be "body".

Pg. 7 -- In Fig. 6, $\bar{\omega}_\theta$ = .2 and p = 1.1

Pg. 11 - Line 11 of the first paragraph should read "value of $\bar{\omega}_\zeta$ for which ground resonance"

Pg. 15 - The curve in Fig. 20 labeled β, ζ, Θ, k_x = 0.2, η_ζ = 0.005 should be β, ζ, Φ, k_x = 0.2, η_ζ = 0.005

AEROMECHANICAL STABILITY OF SOFT INPLANE HINGELESS ROTOR HELICOPTERS

Robert A. Ormiston
Research Scientist

Ames Directorate, Air Mobility R&D Laboratory
U.S. Army Aviation R&D Command
Moffett Field, California

SUMMARY

The fundamental characteristics of air and ground resonance stability of hingeless rotor helicopters are studied in the hover and ground contact conditions. Beginning with Coleman's classical 3 degree-of-freedom articulated rotor system operating *in vacuo*, the effects of additional degrees of freedom, structural damping, aerodynamics, collective pitch, and aeroelastic couplings are introduced and analyzed in a systematic manner. The effects of rotor flapping stiffness significantly influence hingeless rotor aeromechanical stability and can either stabilize or destabilize the system depending on the particular configuration and operating condition. Structural damping is generally stabilizing but certain unusual combinations of body and blade damping can be destabilizing. Aeroelastic couplings contribute moderate stabilizing effects for ground resonance and offer significant benefits for air resonance. Without aeroelastic couplings, matched stiffness configurations are found to be inherently less stable than non-matched stiffness configurations.

1. Introduction

One of the main reasons for the development of hingeless rotors is the simplicity gained by eliminating blade articulation hinges and lead-lag dampers. Soft inplane configurations usually have weight and stress advantages over stiff inplane configurations, and soft inplane rotors are also less susceptible to certain blade flap-lag instabilities. The major disadvantage of the soft inplane rotor is that it may experience coupled rotor-body aeromechanical instabilities termed ground and air resonance. Classical ground resonance was encountered early in the development of the articulated rotor helicopter but air resonance has only become a serious concern since the advent of the hingeless rotor helicopter. Both of these phenomena are more difficult to predict analytically for hingeless rotorcraft than is ground resonance in articulated rotorcraft because of strong aerodynamic and structural couplings inherent in hingeless rotors. Recent full-scale development programs have reflected the complexity of these aeromechanical stability phenomena. For example, of six different hingeless rotor helicopters — the Westland WG-13 Lynx, the Westland Research Scout, the MBB BO-105, Boeing Vertol YUH-61A, Aérospatiale SA 340 Gazelle, and the Lockheed matched stiffness XH-51A — only two were successfully developed or tested without requiring installation of auxiliary lead-lag dampers. The reasons for this wide variation in stability characteristics are not very well understood.

Most research on air-ground resonance falls into two nearly distinct categories. Research on ground resonance originated with the classical work of Coleman[1] who considered a highly simplified analytical model. This model ignored rotor aerodynamics entirely but was quite satisfactory for articulated

Paper presented at the Third European Rotorcraft and Powered Lift Aircraft Forum, Aix-en-Provence, France, September 7-9, 1977.

rotor helicopters and, because of its relative simplicity, was also easy to understand and use for design purposes. In the case of hingeless rotorcraft, additional rotor and fuselage degrees of freedom become important and rotor aerodynamics must be included as well. Most of the remaining research falls in this second category and is more complex and difficult to understand. Nevertheless, some quite good mathematical models[2-4] for hingeless rotorcraft ground and air resonance have been developed and many of the basic characteristics of the problem are now understood. Progress to date, however, has not been sufficient to explain the widely varying experience with the aircraft developments cited above, nor does it permit the development of future aircraft with assurance that such problems can always be avoided. This situation is due, in part, to the fact that most research has concentrated on developing complex mathematical models for predicting stability rather than attempting to break the problem down into simpler elements for the purpose of understanding the underlying characteristics that contribute to the stability of the entire system. What is needed is a third category of research, one of intermediate complexity, to bridge the gap between the classical Coleman analysis and the current highly complex hingeless rotorcraft analyses. In particular, the use of simplified methods is most efficient for parametric analyses of a wide range of configurations. Simplified mathematical models can also be quickly reduced in size to isolate the influence of certain degrees of freedom.

It is the third category of research toward which this paper is directed. The objectives of the paper are to: (1) provide a clearer and more complete understanding of ground-air resonance phenomena; (2) explain some aspects of previous hingeless rotorcraft developments; and (3) identify configurations having favorable stability characteristics. Initial efforts on the last objective were reported in Ref. 5.

2. Mathematical Model

The results presented in this paper are obtained from a simplified mathematical model of a coupled rotor-body system operating in hover or in ground contact. Only those elements required to reasonably represent ground and air resonance phenomena are retained in the analysis. Additional refinements would be necessary to accurately predict the stability of a specific configuration but they would only complicate the present objective of investigating the fundamental characteristics of air and ground resonance phenomena.

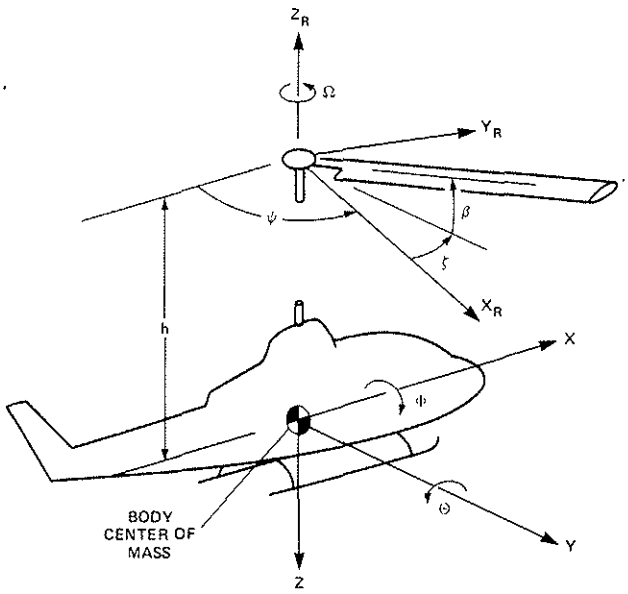

Fig. 1. Physical system for mathematical model.

The mathematical model is based on the physical system sketched in Fig. 1. Symbols and configuration parameters are defined at the end of the paper. The helicopter is composed of a rigid fuselage having pitch and roll rotation (Θ, Φ) about the body center of mass and horizontal translation (X, Y) degrees of freedom in the body fixed X, Y, Z coordinate system. The body physical properties are its mass m_f; pitch and roll inertias I_Y, I_X; landing gear effective stiffnesses in rotation and translation K_θ, K_ϕ, K_Y, K_X; and the distance of the rotor above the body center of mass h. The X_R, Y_R, Z_R coordinate system rotates at a constant angular velocity Ω and is the reference frame for measuring blade deflections. The blades are rigid and rotate against spring restraint about centrally located lead-lag and flap hinges. The blade mass is distributed uniformly along a radial

line with the blade giving equal flap and lead-lag inertias I. The center of mass is at the blade midspan.

The blade flap and lead-lag rotations occur about axes parallel and perpendicular to the plane of rotation, respectively (Fig. 2). The blade flap and lead-lag spring constants are K_β and K_ζ, respectively. The principal elastic axes of flap and lead-lag stiffness do not necessarily coincide with the orientation of the flap and lead-lag hinge axes shown in Fig. 2; this permits structural (elastic) coupling of the blade flap and lead-lag deflections to be introduced. When the blade stiffness principal axes orientation θ_s is zero, the flap and lead-lag deflections are structurally uncoupled and when $\pi/2 > \theta_s > 0$ they are coupled. If θ_s is assumed to be a function of the blade aerodynamic pitch angle θ, different rotor blade and hub types may be simulated. A simple relation used in this paper,

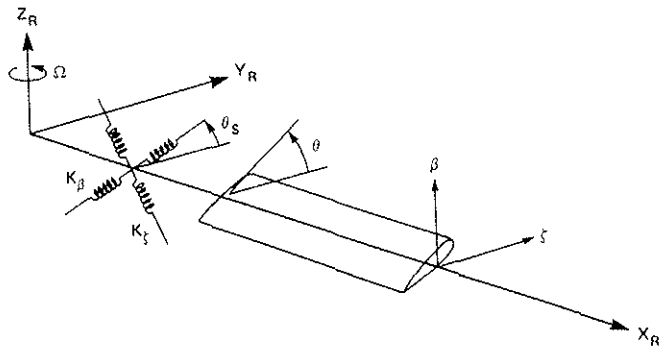

Fig. 2. Details of blade rotations and spring restraint.

$$\theta_s = \theta_{s_o} + R\theta \,, \qquad R = 0 \text{ or } 1 \tag{1}$$

permits the simulation of configurations having bending flexibility located predominantly in the hub, R = 0, or in the blade, R = 1*. The θ_{s_o} term represents flap-lag structural coupling when the blade pitch angle is zero.

The rotor-body physical system consists of a total of 8 degrees of freedom when the individual blade-flap and lead-lag degrees of freedom for b blades (b > 2) are expressed in terms of multiblade coordinates[8] and only the cyclic degrees of freedom (β_c, β_s and ζ_c, ζ_s) are retained. Body vertical translation, yaw rotation, collective flap, and collective lead-lag degrees of freedom are not retained because in hover they are uncoupled from the rotor cyclic and body Θ, Φ, X, Y degrees of freedom and do not participate in ground and air resonance phenomena. For many of the results presented here, even the 8 degree-of-freedom system is not required and a 5 degree-of-freedom system (β_c, β_s, ζ_c, ζ_s, Θ or β, ζ, Θ for short) is sufficient for investigating ground and air resonance behavior.

The equations of motion for this system have been derived using a Newtonian approach. Initially a system of nonlinear equations is obtained and the equations are subsequently linearized by permitting only small perturbation motions about a steady equilibrium operating condition where X_o, Y_o, Θ_o, $\Phi_o = 0$ and β_o, $\zeta_o \neq 0$. This process can be carried out rigorously to yield, for the assumed physical system, an exact set of linear differential equations. Aerodynamic, elastic (blade and landing gear springs), gravitational, and viscous (structural damping), forces and moments are included in the derivation of the equations. For the aerodynamics, a simplified quasi-steady strip theory is employed. A complete derivation of the equations of motion, beyond the scope of this paper, is given in Ref. 9. The final equations are constant coefficient differential equations and the coefficients are functions of the equilibrium flap and lead-lag blade deflections β_o, ζ_o. These are determined by the collective pitch θ and the blade physical properties. The solution of the equations of motion yields the eigenvalues and eigenvectors of the system which yield the desired information regarding the stability characteristics of the system.

*When R = 0 or 1, the present definition of R is equivalent to the one originally presented in Refs. 6 and 7.

The physical system used for the numerical calculations is defined by the following parameter values: $h = 0.4$, $u = 0.1$, $k_y = 0.2$, $\gamma = 5$, $\sigma = 0.05$, $\underline{p} = 1.1$. For ground resonance calculations $\eta_\zeta = \eta_\theta = 0.01$; for air resonance $\bar{\omega}_\theta = \eta_\theta = 0$, $\eta_\zeta = 0.005$. When values different from these are used, they are given in the appropriate figure captions.

3. Classical Ground Resonance

The simplest example of ground resonance involves the lead-lag blade deflections and fuselage horizontal translation in one direction, without any aerodynamic forces. This 3 degree-of-freedom system is denoted in short-hand form as the ζ, X system. Coleman[1] used complex coordinates to describe the blade deflections; here we use multiblade coordinates to write the equations in more conventional form.

$$\begin{bmatrix} 1 & 0 & 0 \\ 0 & 1 & \frac{3}{2} \\ 0 & \frac{\mu}{4} & 1 \end{bmatrix} \begin{Bmatrix} \zeta_c'' \\ \zeta_s'' \\ \frac{X''}{R} \end{Bmatrix} + \begin{bmatrix} 0 & 2 & 0 \\ -2 & 0 & 0 \\ 0 & 0 & 0 \end{bmatrix} \begin{Bmatrix} \zeta_c' \\ \zeta_s' \\ \frac{X'}{R} \end{Bmatrix} + \begin{bmatrix} \bar{\omega}_\zeta^2 - 1 & 0 & 0 \\ 0 & \bar{\omega}_\zeta^2 - 1 & 0 \\ 0 & 0 & \bar{\omega}_X^2 \end{bmatrix} \begin{Bmatrix} \zeta_c \\ \zeta_s \\ \frac{X}{R} \end{Bmatrix} = 0 \qquad (2)$$

The rotor lead-lag multiblade coordinates ζ_c and ζ_s are proportional to the displacement from the center of rotation of the rotor center of mass in the Y and X directions, respectively. In these equations, the body displacement and the lead-lag displacements are coupled in the mass matrix by a term proportional to the rotor mass ratio μ. The system will be unstable when $\bar{\omega}_\zeta < 1$, the rotor and body natural frequencies are near resonance, and when μ is sufficiently large. The condition that $\bar{\omega}_\zeta < 1$ means that the rotor is soft inplane; if $\bar{\omega}_\zeta > 1$ the rotor is termed stiff inplane. Figure 3 illustrates the essential behavior of the system with stability boundaries in the $\bar{\omega}_X$, $\bar{\omega}_\zeta$ plane. Resonance of the system occurs when the uncoupled natural frequencies are equal: $\bar{\omega}_X = 1 - \bar{\omega}_\zeta$. Note that $\bar{\omega}_\zeta$ is the blade natural frequency in the rotating system; in the fixed system it becomes $1 - \bar{\omega}_\zeta$ for the regressing cyclic lead-lag mode and $1 + \bar{\omega}_\zeta$ for the progressing cyclic lead-lag mode. When $\mu = 0$, instability occurs only at resonance, and as μ increases an expanding region of instability develops. This band of instability is narrow for high lead-lag frequencies and broad for low lead-lag frequencies. As the lead-lag frequency increases, the region of instability diminishes until, for stiff inplane rotors, it vanishes completely. Furthermore, within the unstable region, the real part of the unstable eigenvalue becomes progressively larger as $\bar{\omega}_\zeta$ decreases along the resonance line. These basic results lead to the general principle of air and ground resonance that instabilities tend to be more severe at low lead-lag frequencies and less severe at high lead-lag frequencies.

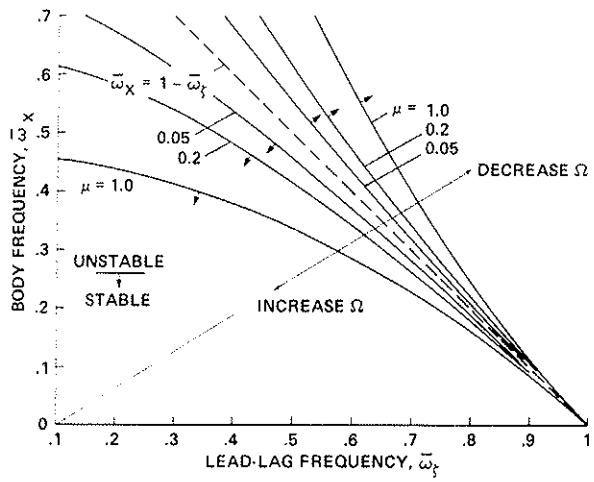

Fig. 3. Classical ground resonance stability boundaries ζ, X degrees of freedom *in vacuo*, without structural damping.

It may be noted that the results in Fig. 3 are presented in an unconventional form. Following the work of Coleman, ground resonance analyses are usually presented in terms of coupled rotor-body system frequencies as a function of rotor rotational speed. Regions of instability are then identified

as areas where frequency coalescences occur. This approach is best suited to studying a particular configuration over a range of rotor speeds. For the present purposes, it is of interest to determine the variation in stability of different classes of configurations as defined by dimensionless parameters such as $\bar{\omega}_X$ and $\bar{\omega}_\zeta$ defined at the normal operating rotor speed. Hence, Fig. 3 is intended to map out a broad spectrum of different rotor-body configurations. In addition, however, it is possible to trace the variation of stability with rotor operating speed for a given configuration. For example, let $\bar{\omega}_{X_o}$ and $\bar{\omega}_{\zeta_o}$ be the dimensionless uncoupled natural frequencies at normal rotor speed Ω_o. Then as Ω varies, the uncoupled frequencies become $\bar{\omega}_X = \bar{\omega}_{X_o}/(\Omega/\Omega_o)$, $\bar{\omega}_\zeta = \bar{\omega}_{\zeta_o}/(\Omega/\Omega_o)$, which defines a straight "operating" line passing through the origin and the nominal operating frequencies $\bar{\omega}_{X_o}$ and $\bar{\omega}_{\zeta_o}$. Increasing the rotor speed is represented by movement along the operating line toward the origin, and decreasing rotor speed moves the frequencies away from the origin along the operating line. Following the example operating line in Fig. 3 illustrates how ground resonance can be encountered by increasing or decreasing rotor speed depending on whether the nominal configuration lies above or below the region of ground resonance instability.

While the ζ, X system of Fig. 3 involved only one body translation degree of freedom, results for a ζ, X, Y system with both X and Y body translation are not qualitatively different. For example, when $\bar{\omega}_X = \bar{\omega}_Y$ the unstable region is broadened slightly. When $\bar{\omega}_X$ is proportional to $\bar{\omega}_Y$, two regions of instability may be present, corresponding to the different frequency coalescences $\bar{\omega}_X = 1 - \bar{\omega}_\zeta$ and $\bar{\omega}_Y = 1 - \bar{\omega}_\zeta$.

4. Rotor-Body Ground Resonance *in vacuo*

The previous simple model with only planar translations is also suitable for articulated rotor helicopters having combined body translation (X, Y) and pitch, roll (Θ, Φ) degrees of freedom. This is because the blade flapping of articulated rotors is only weakly coupled to the body pitch-roll rotations and because the important motions are rotor lead-lag deflections and linear translations at the rotor hub due to pitch and roll of the fuselage. This situation is not true for hingeless rotors where there is strong coupling between rotor flapping motions and body pitch and roll motions. In addition to the mechanical coupling of these degrees of freedom, the rotor flapping also generates large aerodynamic forces on the blades, forces which in turn influence the entire dynamic system.

Before considering the effects of aerodynamics we will first treat the rotor-body system *in vacuo* to identify the effects of rotor flap degrees of freedom and flap hinge restraint stiffness. The body translation degrees of freedom are not required because pitch and roll rotations generate local translations at the rotor hub. Retaining only pitch rotation, the system is denoted β, ζ, Θ and the equations of motion *in vacuo* are:

$$\begin{bmatrix} 1 & 0 & 0 & 0 & -1 \\ 0 & 1 & 0 & 0 & 0 \\ 0 & 0 & 1 & 0 & 0 \\ 0 & 0 & 0 & 1 & -\frac{3}{2}h \\ -1 & 0 & 0 & -\frac{3}{2}h & 1 \end{bmatrix} \begin{Bmatrix} \beta_c'' \\ \beta_s'' \\ \zeta_c'' \\ \zeta_s'' \\ \Theta'' \end{Bmatrix} + \begin{bmatrix} 0 & 2 & 0 & 0 & 0 \\ -2 & 0 & 0 & 0 & 2 \\ 0 & 0 & 0 & 2 & 0 \\ 0 & 0 & -2 & 0 & 0 \\ 0 & -2 & 0 & 0 & 0 \end{bmatrix} \begin{Bmatrix} \beta_c' \\ \beta_s' \\ \zeta_c' \\ \zeta_s' \\ \Theta' \end{Bmatrix} + \begin{bmatrix} p^2-1 & 0 & 0 & 0 & 0 \\ 0 & p^2-1 & 0 & 0 & 0 \\ 0 & 0 & \bar{\omega}_\zeta^2-1 & 0 & 0 \\ 0 & 0 & 0 & \bar{\omega}_\zeta^2-1 & 0 \\ 0 & 0 & 0 & 0 & \frac{2I_\theta}{bI}\bar{\omega}_\theta^2 \end{bmatrix} \begin{Bmatrix} \beta_c \\ \beta_s \\ \zeta_c \\ \zeta_s \\ \Theta \end{Bmatrix} = 0 \qquad (3)$$

The equations for the ζ, Θ degrees of freedom are similar in form to the ζ, X degrees of freedom, Eq. (2). The effect of inertial coupling is now dependent on body geometric and inertia parameters h and k_Y in addition to μ. The rotor flap degrees of freedom couple with body pitch only when $p > 1.0$ and coupling between rotor flap and lead-lag motions occurs only indirectly through

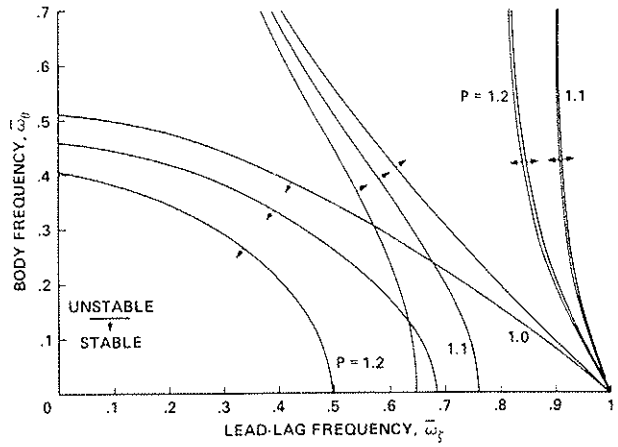

Fig. 4. Effect of flapping stiffness on rotor-body ground resonance *in vacuo*, β, ζ, Θ degrees of freedom, $\mu = 0.1$, $\eta_\zeta = \eta_\theta = 0$.

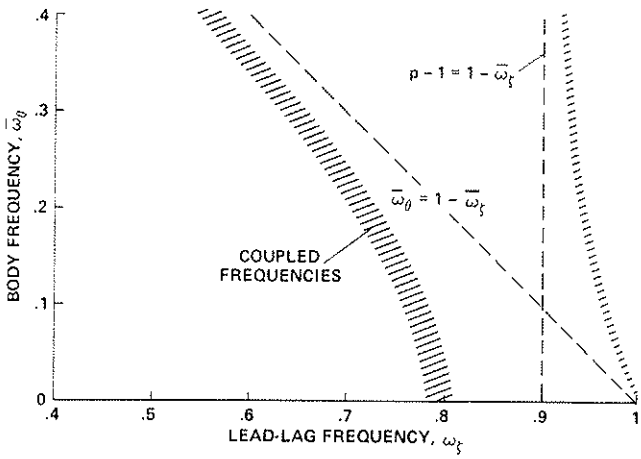

Fig. 5. Resonance frequency conditons for the β, ζ, Θ rotor-body system, $p = 1.1$.

body pitch motion. Typical results for the β, ζ, Θ system are shown in Fig. 4 for several different values of the blade flap frequency p. When $p = 1.0$, the system represents an articulated rotor without rotor flap-body pitch coupling. The stability boundaries are virtually identical to the ζ, X system except for differences in the definition of $\bar{\omega}_\theta$ and $\bar{\omega}_X$.

When flapping stiffness is introduced, $p > 1.0$, the rotor becomes coupled to the pylon by the blade flapping springs resulting in two coupled, rotor flap-body pitch modes. Both of these modes may couple with the regressing lead-lag mode. The first mode is the primary ground resonance mode that derives from the uncoupled body pitch mode $\bar{\omega}_\theta$ and the second mode is a new mode that derives from the uncoupled $p - 1$ flap regressing mode. The resonances of these two modes with the regressing lead-lag mode is shown in Fig. 5 in the $\bar{\omega}_\theta$, $\bar{\omega}_\zeta$ plane for $p = 1.1$. The uncoupled frequency resonances $\bar{\omega}_\theta = 1 - \bar{\omega}_\zeta$ and $p - 1 = 1 - \bar{\omega}_\zeta$ yield straight lines but the coupled frequencies yield approximate resonance bands sketched in Fig. 5.

Both of the frequency resonances produce mechanical instability *in vacuo* but instability due to the higher $\bar{\omega}_\zeta$ resonance band is very weak compared to the lower $\bar{\omega}_\zeta$ resonance band. It is usually unstable only in the absence of aerodynamics and structural damping. The lower $\bar{\omega}_\zeta$ resonance band produces the important ground resonance instability. At high values of $\bar{\omega}_\theta$ it is only slightly affected by rotor flap stiffness, but at low values of $\bar{\omega}_\theta$ flap stiffness is more significant. In the case of very low $\bar{\omega}_\theta$ values, the rotor flap stiffness will be stronger than the body stiffness (landing gear) and the ground resonance mode will begin to assume the character of air resonance instability. In the limit as $\bar{\omega}_\theta \to 0$ in Fig. 4, the low $\bar{\omega}_\zeta$ mechanical instability is essentially air resonance *in vacuo*. Comparing the results in Fig. 4 for different values of p indicates that increasing p generally stabilizes the system by reducing the lead-lag frequency above which ground resonance cannot occur, but destabilizes it by broadening the region of instability. The lower boundary of the unstable region is also shifted to significantly lower values of body pitch frequency. The effects of flap stiffness are therefore dependent on specific values of other configuration parameters and simple generalizations are difficult to make.

Another way of observing the frequency coalescence and mechanical stability behavior is to plot the frequency and damping as a function of lead-lag frequency for a given value of body pitch frequency. A typical result is shown in Fig. 6; coupled and uncoupled frequencies and damping are included. It can be seen that the instability associated with the rotor flap mode is much weaker than the ground resonance instability.

It was noted in Ref. 5 that flap-lag structural coupling has a significant destabilizing effect on ground resonance of hingeless rotorcraft *in vacuo*. Figure 7 illustrates some typical results as θ_{s_0} varies for p = 1.1. The broadening of the region of instability as θ_{s_0} increases confirms the earlier result. The effect of flap-lag structural coupling can become very pronounced for some configurations. When both body pitch and roll rotations are included, and the body pitch and roll inertias are small and equal to each other, the destabilizing effects are very large. One stability boundary included in Fig. 7 for the β, ζ, Θ, Φ system shows the region of instability extending beyond $\bar{\omega}_\zeta = 1.0$ to stiff inplane configurations. Also, the separate instability region associated with the $p - 1 = 1 - \bar{\omega}_\zeta$ resonance is no longer present.

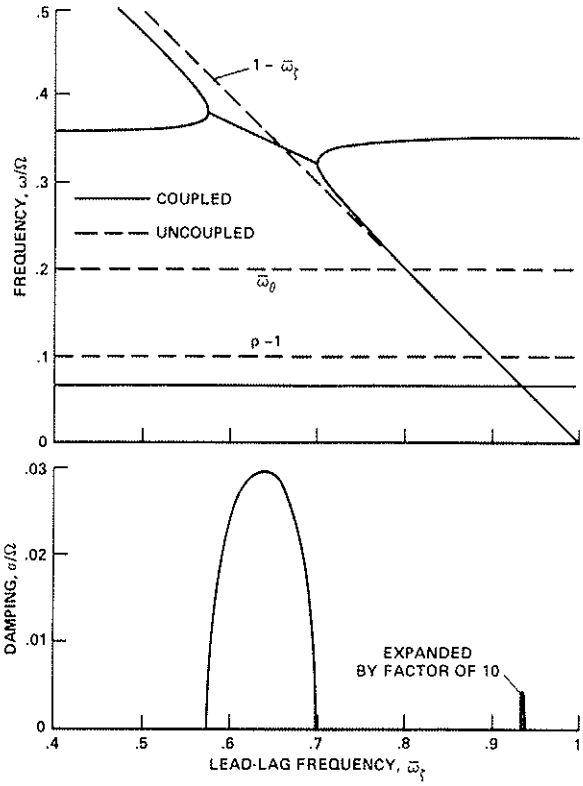

Fig. 6. Frequency and damping of rotor-body system vs lead-lag frequency, β, ζ, Θ degrees of freedom, *in vacuo*, $\eta_\zeta = \eta_\theta = 0$.

5. Rotor-Body Ground Resonance *in vacuo* with Structural Damping

Without aerodynamics or structural damping, ground resonance occurs only as a result of inertial and elastic forces. With the addition of structural damping, the stability of the system becomes considerably more complex and the problem becomes an important subclass of the more general ground and air resonance problem. It is important for two reasons: first, structural damping itself plays an important direct role in the general problem; and second, some of the effects of aerodynamics can be understood more readily if they are considered in terms of equivalent structural damping behavior.

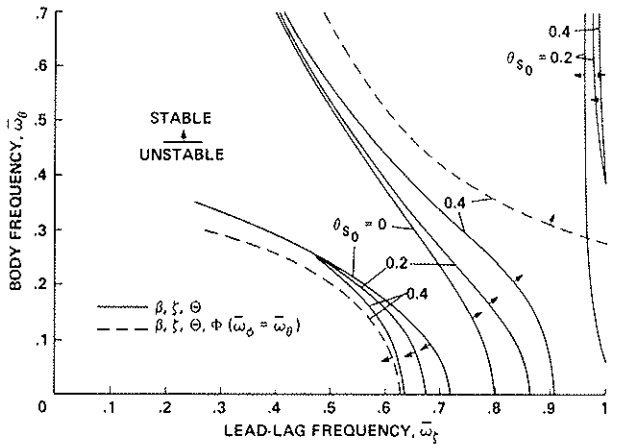

Fig. 7. Effect of flap-lag structural coupling on rotor-body ground resonance *in vacuo*, β, ζ, Θ and β, ζ, Θ, Φ degrees of freedom, $\mu = 0.2$, $p = 1.05$, $\eta_\zeta = \eta_\theta = 0$.

In the present investigation, it was found that the effects of structural damping can lead to very unusual and subtle changes in mechanical stability characteristics. A complete discussion of these changes is beyond the scope of this paper; therefore, only the most pertinent results will be presented. It may be noted that the effects of structural damping (or equivalent viscous damping) on the classical ground resonance problem (ζ, X, Y) have been studied by Coleman.[1] The present investigation is aimed at the slightly more general rotor-body problem (β, ζ, Θ) which includes body-pitch and rotor-flap coupling dynamics of a hingeless rotor configuration.

One of the characteristics of structural damping is that the qualitative behavior of the rotor depends strongly on the relative damping of the blade lead-lag motion compared to the damping of the body motion. When the ratio of blade damping to body damping is near unity or less, the effects of structural damping are relatively straightforward; but when the ratio of blade damping to body damping is sufficiently large, unusual behavior generally occurs. Figures 8-10 give results for a range of different damping configurations. In Fig. 8, the blade lead-lag structural damping and body-pitch structural damping are equal. Blade-flap structural damping is not included. As the level of damping increases, the unstable region in the $\bar{\omega}_\theta$, $\bar{\omega}_\zeta$ plane is reduced compared to the zero damping configuration. Note that the boundary generally recedes along the $\bar{\omega}_\theta$, $1 - \bar{\omega}_\zeta$ resonance line to lower $\bar{\omega}_\zeta$ values as damping increases. There are some unusual characteristics, however. For very low $\bar{\omega}_\theta$ values, structural damping is destabilizing as evidenced by the broadening of the unstable region as $\bar{\omega}_\theta \to 0$. This is caused by the combined structural damping

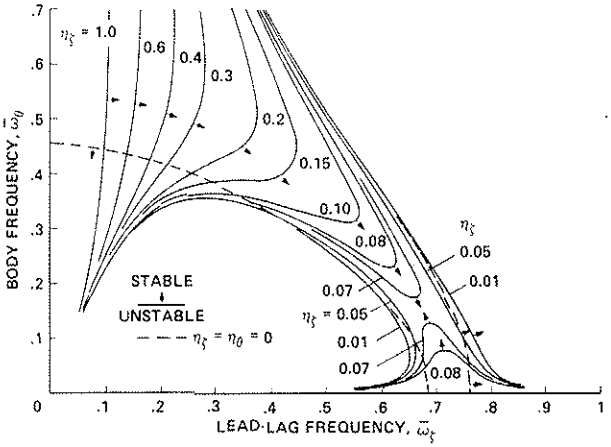

Fig. 8. Effect of structural damping on rotor-body ground resonance *in vacuo*, β, ζ, Θ degrees of freedom, $\eta_\theta = \eta_\zeta$.

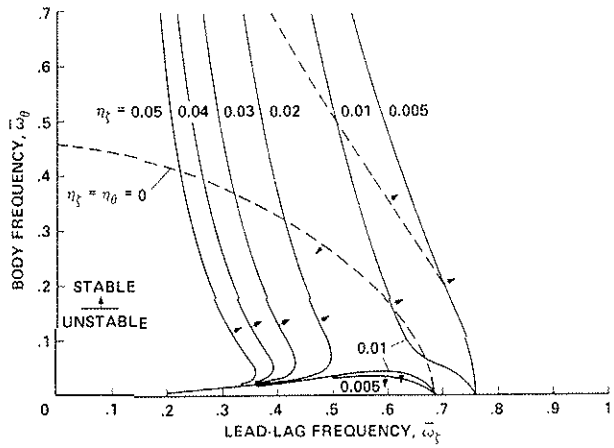

Fig. 9. Effect of structural damping on rotor-body ground resonance *in vacuo*, β, ζ, Θ degrees of freedom, $\eta_\theta = 100\ \eta_\zeta$.

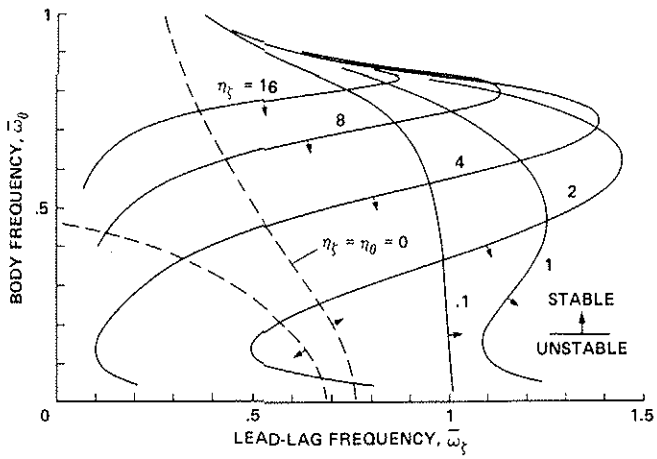

Fig. 10. Effect of structural damping on rotor-body ground resonance *in vacuo*, β, ζ, Θ degrees of freedom, $\eta_\theta = 0.001\ \eta_\zeta$.

of body pitch and rotor flap motions becoming vanishingly small as $\bar{\omega}_\theta \to 0$, this is because the total body damping ($2\eta_\theta\bar{\omega}_\theta\theta'$) goes to zero, even when the damping ratio $\eta_\theta \neq 0$, and because flap structural damping is not included. Thus, the ratio of blade lead-lag damping to flap and pitch damping becomes infinite, leading to a condition where unusual destabilizing behavior occurs. Typically, it is found that when either η_ζ or η_θ is zero and the other is nonzero, the system will be unstable for any combination of $\bar{\omega}_\theta$ and $\bar{\omega}_\zeta$. This is not necessarily of practical concern, however, since it is impossible to have zero structural damping in a real physical system. The instability region associated

with the $p - 1 = 1 - \bar{\omega}_\zeta$ resonance is eliminated by very small amounts of structural damping and is therefore not included in Figs. 8-10.

Figure 9 illustrates the stability of configurations having small blade lead-lag damping and large body pitch damping. Because of the large difference in η_ζ and η_θ, some regions are destabilized in comparison to the configurations without any structural damping. This particular damping combination is analogous to the more complete problem including aerodynamics where rotor flap aerodynamic damping moments produce a large effective body-pitch damping for hingeless rotor configurations. The last result in Fig. 10 is intended to illustrate the extreme effects of structural damping for very unusual configurations. In this case, the body-pitch damping is extremely small in comparison to the blade lead-lag damping. It is observed that as the damping increases, instabilities of stiff inplane configurations are produced. It should be emphasized that this is not of great practical significance but it is an interesting and unusual mathematical result.

6. Rotor-Body Ground Resonance with Aerodynamics

We now continue to generalize the physical system by including rotor aerodynamic forces. The zero collective pitch operating condition is the simplest case because many of the aerodynamic terms in the equations vanish for $\theta = 0$. The first results are given in Fig. 11 for the typical $p = 1.1$ configuration with equal blade inplane and body-pitch structural damping. The blade Lock number and rotor solidity are 5 and 0.05, respectively. The stability boundaries are well-behaved, receding continuously with increasing structural damping, but a few details deserve comment. First, with zero structural damping, the effects of aerodynamics alone are strongly destabilizing compared to the undamped configuration *in vacuo*. This is the result of an unfavorable effective damping combination where the blade aerodynamic lead-lag damping is very small and the body aerodynamic damping is very large, similar to Fig. 9. Only a small amount of blade lead-lag structural damping is required to rectify this imbalance and the stability boundary quickly recedes. It is also evident that the high $\bar{\omega}_\theta$, $\bar{\omega}_\zeta$ portion of the boundary is much less sensitive to structural damping than the lower $\bar{\omega}_\theta$, $\bar{\omega}_\zeta$ boundary.

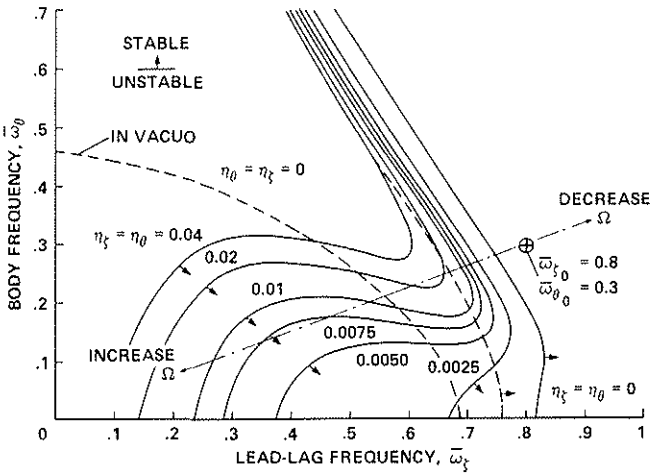

Fig. 11. Effect of aerodynamics and structural damping on rotor-body ground resonance, β, ζ, Θ degrees of freedom, $\eta_\theta = \eta_\zeta$, $\theta = 0$.

It should be noted that stability variations for rotor speed changes can be only approximately inferred from Fig. 12 when $p > 1.0$. Rotor speed operating lines passing through the origin define the body pitch and blade lead-lag frequency variations but not the flap frequency variations as p varies with Ω.

$$p = \sqrt{1 + (p_o^2 - 1)/(\Omega/\Omega_o)^2} \tag{4}$$

Nevertheless, one may still infer the general effects of rotor speed variations near the nominal configuration point $\bar{\omega}_{\theta_o}$, $\bar{\omega}_{\zeta_o}$, by ignoring the small shift in the stability boundary location as p changes with Ω/Ω_o. In particular, it can be appreciated that a practical concern would be nominal design configurations having rotor speed operating lines crossing the "nose" (high $\bar{\omega}_\zeta$, low $\bar{\omega}_\theta$)

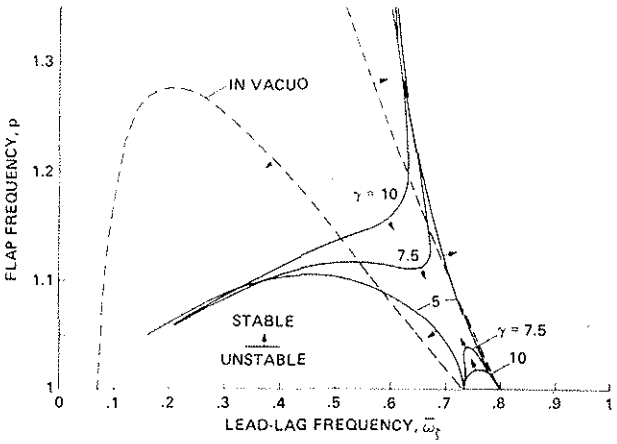

Fig. 12. Effect of flapping stiffness and Lock number on rotor-body ground resonance, β, ζ, θ degrees of freedom, $\bar{\omega}_\theta = 0.2$, $\theta = 0$.

of the stability boundaries in Fig. 11. For example, ignoring the effect of small p variations with Ω, a nominal configuration with $\bar{\omega}_{\zeta_o} = 0.8$, $\bar{\omega}_{\theta_o} = 0.3$, and 1% blade and body structural damping ($\eta_\zeta = \eta_\theta = 0.01$) would cross into the unstable region with a slight increase in rotor speed, and then become stable again as rotor speed increased further.

An important characteristic of hingeless rotors is the high angular rate damping of the coupled rotor-body system produced by aerodynamic forces acting on the blades that are transferred to the body by the flapping stiffness of the rotor. The body-mode damping increases in proportion to the flapping stiffness which in turn is generally defined in terms of the uncoupled blade-flap frequency $p = \sqrt{1 + K_\beta/I\Omega^2}$ where K_β is the spring restraint stiffness of the idealized centrally hinged rigid blade. Previous investigations have concluded that the effective body damping of a hingeless rotorcraft generally contributes a favorable stabilizing effect for air and ground resonance phenomena. Because of their importance, we will consider the effects of blade-flap stiffness and aerodynamic damping in more detail. Two results, at zero collective pitch, will be considered.

The first result, Fig. 12, is a comparison of *in vacuo* and in air stability boundaries in the p, $\bar{\omega}_\zeta$ plane for a body-pitch frequency of $\bar{\omega}_\theta = 0.2$. In this plot, the basic *in vacuo* mechanical instability is centered in the $\bar{\omega}_\theta$, $1 - \bar{\omega}_\zeta$ resonance. For $p = 1.0$, this occurs when $1 - \bar{\omega}_\zeta \approx \bar{\omega}_\theta = 0.2$ or $\bar{\omega}_\zeta \approx 0.8$, but as p increased above 1.0, the rotor flap stiffness increases the coupled rotor-body pitch frequency and lowers the lead-lag frequency for resonance. This explains the shift of the instability region to lower $\bar{\omega}_\zeta$ as p increases. The region of instability at very low $\bar{\omega}_\zeta < 0.1$ is due to the effects of structural damping. The effect of aerodynamics is examined by increasing the Lock number from zero (*in vacuo*) to 10. It is assumed that the blade mass and inertia properties are held constant and that the Lock number is increased by increasing the air density or the blade chord. For $\gamma = 5$ the instability region, compared to the *in vacuo* case, is reduced for low p, high $\bar{\omega}_\zeta$ values near the frequency resonance, but is expanded for low $\bar{\omega}_\zeta$ configurations. It may be pointed out that the reduction of stability for these low $\bar{\omega}_\zeta$ configurations is relatively unimportant compared to the increased stability for the higher $\bar{\omega}_\zeta$ configurations. As the Lock number increases, it is apparent that the system is further stabilized by rotor aerodynamic flap damping in the vicinity of the $1 - \bar{\omega}_\zeta \approx \bar{\omega}_\theta$ resonance.

Figure 12 also illustrates that both aerodynamic flap damping (Lock number) and rotor flap stiffness p are important in determining hingeless rotor stability. For very low values of p, the rotor aerodynamic flap damping cannot be effectively transferred to the body due to low blade flap stiffness. This explains the small region of instability that remains for $\gamma = 10$ at very low values of p. In fact as $p \to 1.0$, the in-air and *in vacuo* stability boundaries are nearly coincident, indicating that aerodynamics has a negligible effect on articulated rotor ground resonance. Figure 12 also indicates that too large an increase in p can lead to ground resonance instability. This is because the underlying mechanical instability becomes stronger — as p increases and $\bar{\omega}_\zeta$ decreases along the resonance line — and the aerodynamic flap damping is not sufficient to suppress it.

The second result compares ground resonance stability boundaries in the $\bar{\omega}_\theta$, $\bar{\omega}_\zeta$ plane for several different values of p. Figure 13 illustrates that flap stiffness has a moderate beneficial influence on the upper part of the stability boundaries. Increasing flap frequency stabilizes the "nose" of the stability boundaries by significantly lowering the maximum value for which ground resonance can occur. The lower portions of the boundaries are much more sensitive to p and increasing p generally enlarges the region of instability. This is primarily due to the increasingly strong mechanical instability that is produced by high values of flap stiffness at low body frequencies, as was evident in the *in vacuo* stability boundaries in Figs. 4 and 12. For these configurations, the rotor aerodynamic flap damping is insufficient to suppress the underlying mechanical instability.

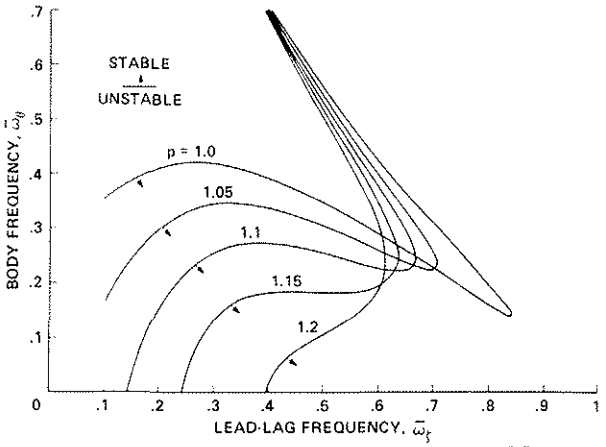

Fig. 13. Effect of flapping stiffness on rotor-body ground resonance, β, ζ, Θ degrees of freedom, $\eta_\zeta = \eta_\theta = 0.02$, $\theta = 0$.

The next step is to examine the influence of collective pitch on the ground resonance instability. The configuration in Fig. 11 that had 1% structural damping is presented in Fig. 14 for several values of collective pitch. It is clear that the additional aerodynamic coupling effects are generally destabilizing, particularly in lowering the "nose" of the stability boundary. The upper and lower left portions of the boundary are to some extent stabilized, however. It is not possible, within the scope of this paper, to determine the precise reasons for the destabilizing influence of collective pitch. The discussion in Ref. 4 indicates that combined effects of collective pitch, induced inflow, and inertial coupling due to equilibrium flap and lead-lag displacements β_0, ζ_0 of the blade all contribute in a complex way. A more complete understanding of Fig. 14 and other stability characteristics described in this paper must be left for future investigation.

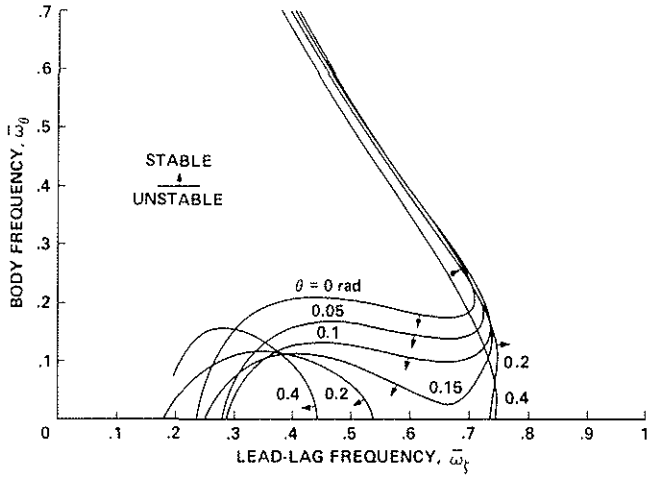

Fig. 14. Effect of collective pitch on rotor-body ground resonance, β, ζ, Θ degrees of freedom.

7. Rotor-Body Ground Resonance with Aeroelastic Couplings

The previous results for rotor-body ground resonance in air have not included any rotor blade aeroelastic couplings such as kinematic pitch-lag coupling, or flap-lag structural coupling. These couplings arise in actual rotor blades as a consequence of the distribution of bending and torsion stiffness along the radius and as a consequence of configuration details of the rotor hub and the blade pitch control system. It is possible to control the magnitude of the rotor blade aeroelastic couplings by applying suitable techniques in the design of the rotor. Moreover, it is well known that aeroelastic couplings can strongly influence a wide range of aeroelastic behavior of hingeless rotors

including ground and air resonance stability characteristics. However, not as well known are some of the details that determine which couplings are stabilizing or destabilizing for air and ground resonance, and how strong these effects are for different hingeless rotorcraft configurations.

While the present analysis is not capable of treating the coupled elastic bending and torsion motions of actual hingeless rotor blades, the introduction of representative kinematic pitch-flap, pitch-lag, and structural flap-lag couplings allows a fairly general investigation to be conducted of aeroelastic coupling effects. The relationship between actual elastic blade properties and the effective aeroelastic coupling parameters applicable to an idealized rigid blade analysis is discussed in Refs. 10 and 11. Space limitations do not permit the inclusion here of a large number of results and only a summary of the most important ones is presented. Two operating conditions at collective pitch values of $\theta = 0$ and 0.3 rad will be considered. Figure 15 presents the zero pitch angle results and compares the effects of pitch-lag coupling θ_ζ, flap-lag structural coupling, θ_s and combined pitch-lag and flap-lag coupling with the baseline configuration having no aeroelastic couplings. First, pitch-lag coupling alone is not beneficial in the important regions of the $\bar{\omega}_\theta$, $\bar{\omega}_\zeta$ plane; that is, near the "nose" region of the stability boundary. It is beneficial near the lower boundary but that is a relatively unimportant region. Neither is flap-lag structural coupling θ_s beneficial; in fact, it is highly destabilizing in important regions of the $\bar{\omega}_\theta$, $\bar{\omega}_\zeta$ plane. The combination of both couplings is not particularly beneficial either, falling roughly between the effects of the individual couplings.

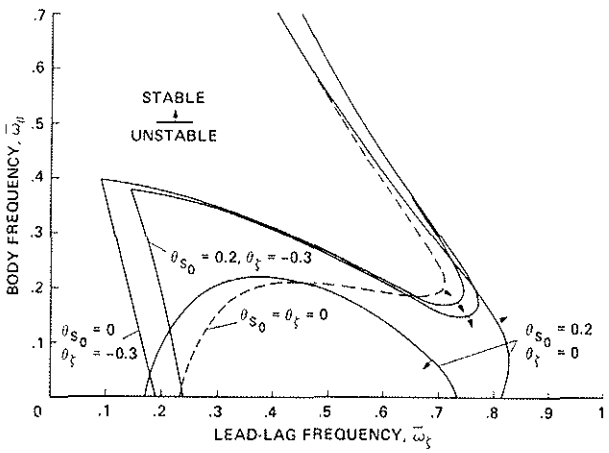

Fig. 15. Effect of aeroelastic couplings on rotor-body ground resonance at zero collective pitch, β, ζ, Θ degrees of freedom.

The region of instability for the baseline configuration is greatly enlarged when the collective pitch angle is increased above zero. In this case, the aeroelastic couplings prove to be far more beneficial. As shown in Fig. 16, pitch-lag coupling is highly stabilizing, but for the configuration shown, $p = 1.1$, $\eta_\zeta = \eta_\theta = 0.01$, the improvement would not be sufficient for moderately large values of body pitch frequency. The addition of flap-lag structural coupling enhances the effect of pitch-lag coupling and produces a further substantial reduction in the region of instability, particularly in the important "nose" region. While favorable effects can be obtained with aeroelastic couplings for the rotor thrusting condition, the specific values of the coupling parameters must be carefully chosen. It is possible to worsen ground resonance instability with certain combinations of couplings or with excessive amounts of coupling. In Fig. 17, for example, the upper

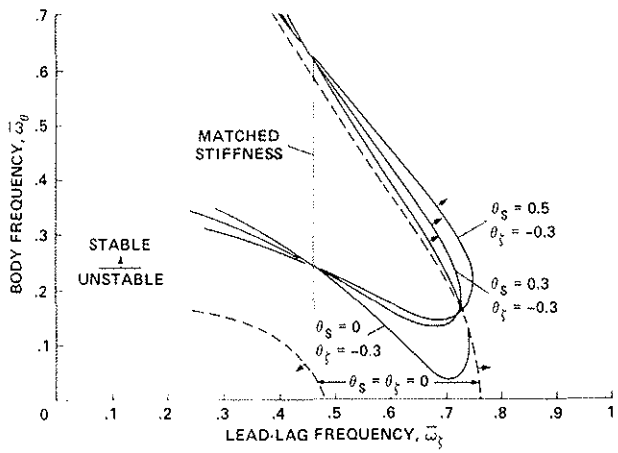

Fig. 16. Effect of aeroelastic couplings on rotor-body ground resonance at nonzero collective pitch, β, ζ, Θ degrees of freedom, $\theta = 0.3$.

boundary of the unstable region expands for large values of flap-lag structural coupling.

These results illustrate the potential benefits to the ground resonance problem that may be obtained at nonzero collective pitch angles. The lack of favorable effects at zero pitch angle confirms earlier preliminary findings reported in Ref. 5.

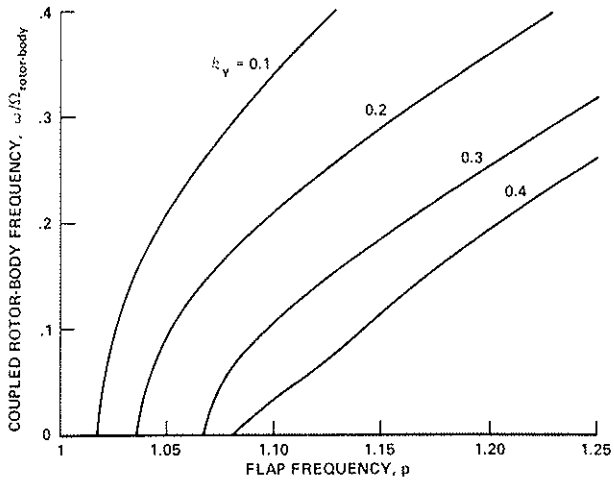

Fig. 17. Frequencies of coupled rotor-body system in air, β, Θ degrees of freedom, θ = 0.

8. Air Resonance

Air resonance is usually considered to be an aeromechanical instability of an airborne rotorcraft that occurs as a result of resonance between the regressing lead-lag mode and a rotor-body coupled pitch or roll mode. As such it involves rigid body translation degrees of freedom of the fuselage and aerodynamic forces associated with a thrusting rotor. Since the helicopter is not restrained by ground contact, the rotor-body pitch or roll mode is a "free-free" mode where rotor flapping and body rotation react against each other as mass elements joined by the rotor blade flapping springs. The coupled rotor-body frequency is determined by the mass, inertia, stiffness, and geometric parameters of the rotor and the body. An example of the frequency variation with these parameters is shown for the simple rotor flap-body pitch (β, Θ) system in Fig. 17. For simplicity, the body translation (X) degree of freedom is omitted. The coupled rotor-body mode derives mainly from the (p - 1) regressing rotor flap mode and thus its frequency is a strong function of the blade flapping stiffness and hence p. As p is decreased to 1.0 (articulated blade), the rotor and body become uncoupled and the rotor regressing mode assumes its uncoupled fixed system frequency p - 1.0 = 0. The coupled rotor-body frequency is also a strong function of the body pitch inertia parameter k_y, and increasing inertia lowers the coupled frequency.

Because the coupled rotor-body frequency is a direct function of blade flap frequency, the condition for resonance between a rotor-body pitch or roll frequency and the regressing lead-lag frequency is most conveniently depicted in the p, $\bar{\omega}_\zeta$ plane. The mechanical stability resonance can be obtained by setting the rotor-body pitch-mode frequency of Fig. 17 equal to the regressing lead-lag frequency; that is, $\bar{\omega}_{\text{rotor-body}} = 1 - \bar{\omega}_\zeta$ for each value of p. This procedure yields a resonance line in the p, $\bar{\omega}_\zeta$ plane that is the air resonance counterpart of the $\bar{\omega}_\theta = 1 - \bar{\omega}_\zeta$ resonance line in the $\bar{\omega}_\theta$, $\bar{\omega}_\zeta$ plane for ground resonance. The only difference is that the ground resonance line is a straight line, whereas the air resonance line is not.

The first air resonance stability boundaries in the p, $\bar{\omega}_\zeta$ plane are given in Fig. 18 for the flap, lead-lag, and body pitch (β, ζ, Θ) system. The body X translation degree of freedom is omitted for simplicity; it will be shown that this has a very small effect on the air resonance stability boundaries. Figure 18 first shows a stability boundary for the rotor-body system *in vacuo* without lead-lag structural damping to illustrate the basic mechanical instability underlying air resonance. It is evident that the instability is associated with a $\bar{\omega}_{\text{rotor-body}} = 1 - \bar{\omega}_\zeta$ resonant frequency line as discussed above. This should be compared to the ground resonance case in Fig. 3. It is also interesting that the air resonance can be roughly interpreted as a limiting case of ground resonance where the uncoupled body frequency $\bar{\omega}_\theta$ goes to zero. For the simple system being studied here, the results given for the *in vacuo* case in

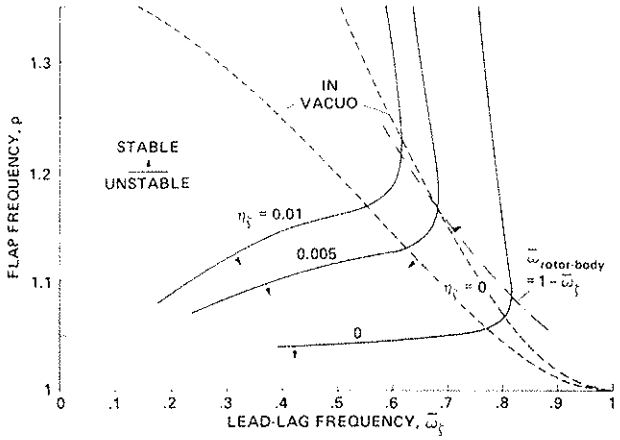

Fig. 18. Effect of aerodynamics and structural damping on air resonance stability, β, ζ, Θ degrees of freedom, $\theta = 0$.

Fig. 18 are, in fact, identical to the results on the abscissa of Fig. 4 where $\bar{\omega}_\theta = 0$.

The "in air" air resonance stability boundaries in Fig. 18 are given for the somewhat artificial zero collective pitch condition. When lead-lag structural damping is zero, the lead-lag damping due to aerodynamic drag is very small, and the body damping is large due to coupling with rotor aerodynamic flap damping. (This is similar to the *in vacuo* results in Fig. 9 where the body structural damping was much larger than the blade lead-lag damping.) With $\eta_\zeta = 0$, the aerodynamic damping is quite destabilizing for the upper and lower stability boundaries compared to the *in vacuo* result, except for a small range of high lead-lag frequency $\bar{\omega}_\zeta \gtrsim 0.8$. As lead-lag structural damping is added, the stability boundaries contract significantly and only small amounts of structural damping are required to eliminate air resonance instability at zero blade-pitch angle. As in the case of the *in vacuo* stability boundary, the in-air stability boundaries for the β, ζ, Θ system represent a limiting case of ground resonance, as in Fig. 13 when $\bar{\omega}_\theta = 0$.

Both the *in vacuo* and in-air cases in Fig. 18 illustrate a basic characteristic of air resonance stability, namely, that increasing the flap frequency generally reduces the stability of the system. In particular, following the trend of the resonant frequency line in the p, $\bar{\omega}_\zeta$ plane of Fig. 18, increasing p and decreasing $\bar{\omega}_\zeta$ is highly destabilizing. The higher the flap frequency and the lower the lead-lag frequency, the more lead-lag structural damping is required to prevent air resonance instability.

It is of interest to point out that the p, $\bar{\omega}_\zeta$ plane used for air resonance stability boundaries can be used to define operating lines for rotor speed variations like Fig. 4 and to define certain classes of hingeless rotor configurations. Rotor speed operating lines in the p, $\bar{\omega}_\zeta$ plane are defined by the equations

$$p = \sqrt{1 + (p_o^2 - 1)/(\Omega/\Omega_o)^2} \quad \text{and} \quad \bar{\omega}_\zeta = \bar{\omega}_{\zeta_o}/(\Omega/\Omega_o) \tag{5}$$

where Ω_o, $\bar{\omega}_{\zeta_o}$, and p_o are the nominal rotor speed and blade frequencies at nominal rotor speed, respectively. Several typical operating lines are shown in Fig. 19.

It is also possible to construct curves of constant flap-lag structural coupling in the p, $\bar{\omega}_\zeta$ plane. Flap-lag structural coupling depends on both θ_s and the difference in lead-lag and flap stiffness $K_\zeta - K_\beta$. Expressed in terms of the blade-flap and lead-lag frequencies, the difference in stiffnesses can be written as $\bar{\omega}_\Delta^2 = \bar{\omega}_\zeta^2 - \bar{\omega}_\beta^2$ or $\bar{\omega}_\Delta^2 = 1 + \bar{\omega}_\zeta^2 - p^2$ since $\bar{\omega}_\beta^2 = p^2 - 1$. One configuration of particular interest is the matched stiffness configuration where the flap and lead-lag spring stiffnesses are equal and $\bar{\omega}_\Delta^2 = 0$. A high value of the structural coupling parameter would be $\bar{\omega}_\Delta^2 = 0.43$, corresponding to $\bar{\omega}_\zeta = 0.8$ and $p = 1.1$. Several loci of constant $\bar{\omega}_\Delta^2$ are plotted in Fig. 19. A comparison of Figs. 18 and 19 should make it clear that the closer a configuration is to the matched stiffness configuration, the more likely is the chance of encountering air resonance stability, all other parameters being held constant. Moving from one constant $\bar{\omega}_\Delta^2$ line to a lower value $\bar{\omega}_\Delta^2$ line moves in the direction of more severe air resonance.

The effects of body pitch-roll coupling on air resonance are briefly examined in Fig. 20 for the zero collective pitch condition. Using typical pitch and roll inertia values, the stability of the uncoupled pitch and roll modes are shown for the *in vacuo* and in-air conditions. Note here that the difference in body inertia produces a different resonant frequency line in the p, $\bar{\omega}_\zeta$ plane, with the pitch mode resonance occurring at larger values of $\bar{\omega}_\zeta$ than the roll-mode resonance. Except for the difference in frequency, the pitch- and roll-mode instabilities *in vacuo* are roughly similar. With aerodynamics and lead-lag structural damping included, they are quite different, however. The pitch-mode stability boundary is virtually eliminated, moving to very high values of p, and low values of $\bar{\omega}_\zeta$, while the roll-mode boundary extends down to very low values of p. This difference is essentially a rotor-body inertia ratio effect similar to the mass ratio μ that governs the classical ground resonance illustrated in Fig. 3. With a large pitch inertia, the uncoupled-pitch-mode air resonance becomes a relatively mild instability. In the case of the roll mode, the low body roll inertia is relatively ineffective in opposing instability and roll-mode air resonance is relatively severe. In the case of the fully coupled rotor-body pitch-roll system (β, ζ, Θ, Φ), the roll mode is dominant and the coupled stability boundary is very similar to the uncoupled roll-mode air resonance boundary. In the presence of aeroelastic coupling to be considered below, we will see that the low inertia roll mode is not necessarily always the least stable mode, however.

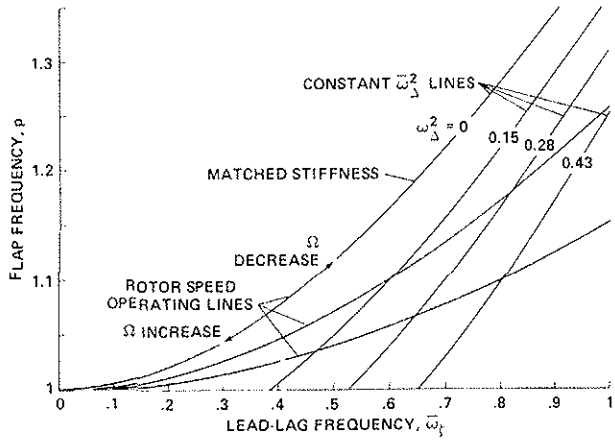

Fig. 19. Rotor speed operating lines and loci of constant flap-lag structural coupling in the p, $\bar{\omega}_\zeta$ plane.

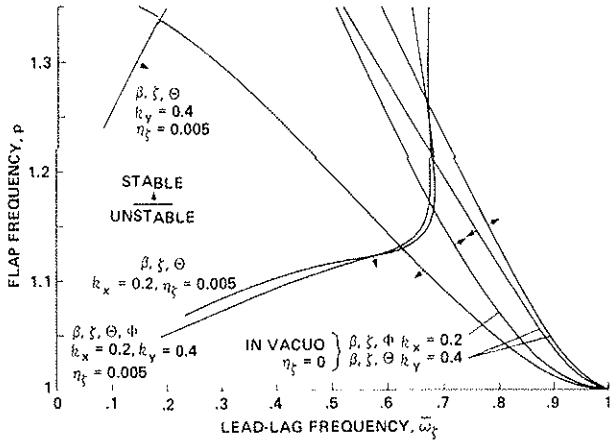

Fig. 20. Effect of body inertia and pitch-roll coupling on air resonance stability, β, ζ, Θ and β, ζ, Θ, Φ degrees of freedom, $h = 0.4$, $\mu = 0.1$, $\theta = 0$.

As in the case with ground resonance, the effects of rotor collective pitch significantly influence air resonance stability. Typical results are shown in Fig. 21. Both the upper and extreme lower $\bar{\omega}_\zeta$ ends of the stability boundary recede with increasing collective pitch but the important "nose" region expands until the instability follows the resonance line down to the $p = 1$ abscissa. Considerable amounts of lead-lag structural damping are required to suppress the air resonance instability at higher blade pitch angles.

It should be noted that rotor speed variation operating lines are only accurate for indicating air resonance stability boundary crossings in the p, $\bar{\omega}_\zeta$ plane when rotor collective pitch is zero, or is invariant with rotor speed. To represent the case of rotor speed variations for a helicopter hovering with a constant rotor thrust, collective pitch would have to vary as a function of rotor speed and the rotor speed operating lines in the p, $\bar{\omega}_\zeta$ plane would have to be used in conjunction with a family of stability boundaries for various collective pitch angles.

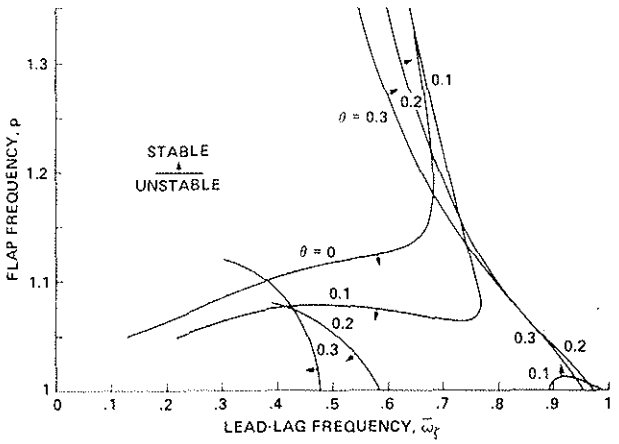

Fig. 21. Effect of collective pitch on air resonance stability, β, ζ, Θ degrees of freedom.

For all the air resonance results presented above, the rotor-body system has been restricted to rotor flap and lead-lag degrees of freedom and body pitch or roll degrees of freedom. As noted above, the effect of body translation does not fundamentally change the air resonance behavior but other modes do appear when body translation is permitted. In the interest of completeness, a case involving body translation is included. The main effect of adding body X translation is the appearance of the low frequency flight dynamic pitch mode (or pitch-roll modes for both X and Y translations). This mode primarily involves coupling between body pitch and translation due to horizontal components of the rotor thrust produced by pitch rotations of the body. Pitch moments are in turn generated by the lifting rotor in response to body translatory velocity. This flight dynamics mode typically is mildly unstable and does not normally couple with the air resonance mode which is of considerably higher frequency. The stability boundaries for two systems, one without X translation (β, ζ, Θ) and the other with X translation (β, ζ, Θ, X), are compared in Fig. 22 for a pitch angle of $\theta = 0.1$ rad. As can be seen, the difference between the two air resonance stability boundaries is very small. A flight dynamics mode stability boundary for the β, ζ, Θ, X system is also shown and indicates that this mode becomes stable at very large flap frequencies, except for $\bar{\omega}_\zeta \approx 1$ when regressing lead-lag frequency approaches coalescence with the flight dynamics mode frequency.

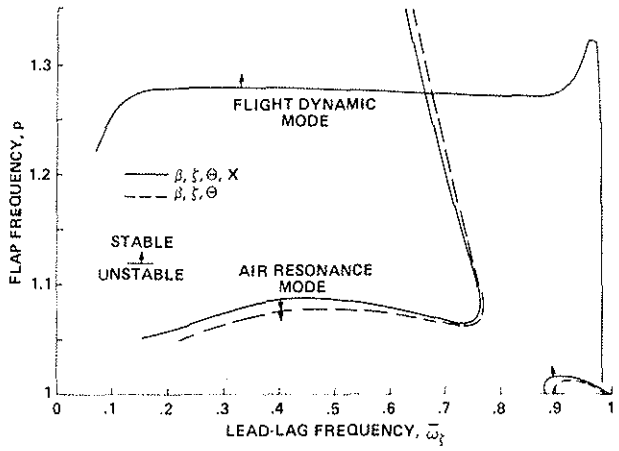

Fig. 22. Effect of body translation on air resonance stability, β, ζ, Θ and β, ζ, Θ, X degrees of freedom, $\theta = 0.1$.

9. Air Resonance with Aeroelastic Couplings

As in the treatment of ground resonance, we will now examine the effects of aeroelastic couplings on air resonance. Stability boundaries for the system at $\theta = 0.2$ rad and different combinations of pitch-lag and flap-lag structural coupling are given in Fig. 23. It is noted that the baseline boundaries without coupling show a wide region of instability. Nearly any rotor speed operating line would be expected to cross into this unstable region. Consider first the effect of flap-lag structural coupling. In contrast to ground resonance results discussed above, and even air resonance at zero pitch angle, this coupling is now seen to be mildly stabilizing in some areas. Also superimposed on this plot is the $p, \bar{\omega}_\zeta$ line for matched stiffness configurations. Since flap-lag structural coupling vanishes for these configurations, the stability boundaries for the two values of θ_s coalesce as they cross the matched stiffness line.

The effect of pitch-lag coupling is also stabilizing but much more so than flap-lag structural coupling alone. Nevertheless, for the parameters

of Fig. 23, the region of instability is probably large enough to produce instability at some point along the rotor speed operating line. The combination of flap-lag structural coupling and pitch-lag coupling proves to be most effective in preventing air resonance instability for the present configuration parameters. This combination affords a wide range of nominal frequency combinations $\bar{\omega}_{\zeta_o}$, p_o that are stable at all points along their rotor speed operating lines (here we ignore the effect of θ variations with Ω). It should be noted that only a few results are presented in Fig. 23 and that many other combinations of aeroelastic couplings exist that can be destabilizing. Also, large amounts of pitch-lag and flap-lag structural coupling are not necessarily more beneficial than small amounts. Excessive amounts may also produce new modes of instability; for example, flap-lag structural coupling together with large negative values of pitch-lag coupling can produce progressing lead-lag mode $(1 + \bar{\omega}_\zeta)$ instability for some configurations. In fact, this mode is unstable for very low $\bar{\omega}_\zeta$ values in Fig. 23.

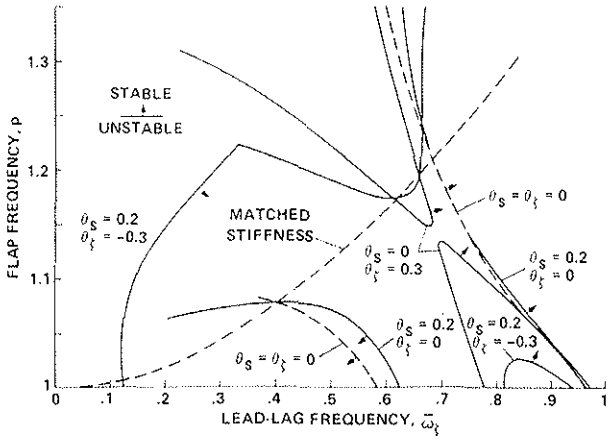

Fig. 23. Effect of aeroelastic couplings on air resonance stability, β, ζ, Θ degrees of freedom, $\theta = 0.2$.

To complete this brief investigation of the effects of aeroelastic couplings on air resonance stability, a comparison will be made of the effects of couplings on the regressing lead-lag mode damping as a function of rotor speed for two different rotor-body configurations. The full 8 degree-of-freedom rotor-body system will be used (β, ζ, Θ, Φ, X, Y), and the rotor thrust will be held constant during rotor speed variations by changing collective pitch angle accordingly. The two different configurations will be a matched stiffness rotor ($\bar{\omega}_{\zeta_o} = 0.5$, $p_o = 1.118$) and a typical nonmatched stiffness rotor ($\bar{\omega}_{\zeta_o} = 0.7$, $p_o = 1.10$). Both rotors have 1/2% critical structural damping for lead-lag motions. Several results for each configuration are presented to illustrate successively the effects of aerodynamics, collective pitch, and aeroelastic couplings. Beginning with the matched stiffness configuration in Fig. 24, the basic mechanical instability is shown by the *in vacuo* result where the pitch and roll modes become unstable as the regressing rotor-mode frequency crosses the body pitch and roll frequencies. The pitch-mode instability is weaker than the roll mode since it occurs at a higher lead-lag frequency and because the pitch inertia is larger than the roll inertia. The frequencies are shown for the *in vacuo* case and one "in air" case. It may be noted that the regressing mode damping in Fig. 24 is given by the real part of the eigenvalue made dimensionless by the rotor speed Ω. The fraction of critical damping can be obtained from the equation

$$\frac{\sigma/\Omega}{\sqrt{(\sigma/\Omega)^2 + (\omega/\Omega)^2}} \tag{6}$$

where ω/Ω is the frequency of the $1 - \bar{\omega}_\zeta$ mode in Fig. 25.

Adding blade structural damping and zero blade pitch aerodynamics to the matched stiffness configuration completely eliminates the weaker pitch-mode instability and stabilizes the roll mode. A weak but broader Ω range roll-mode instability remains, however. When a constant rotor thrust is added corresponding to a collective pitch $\theta_o = 0.15$ at nominal rotor speed, the system becomes unstable over a much wider rotor speed range. It is of interest to note that the damping in the vicinity of the pitch mode appears to increase

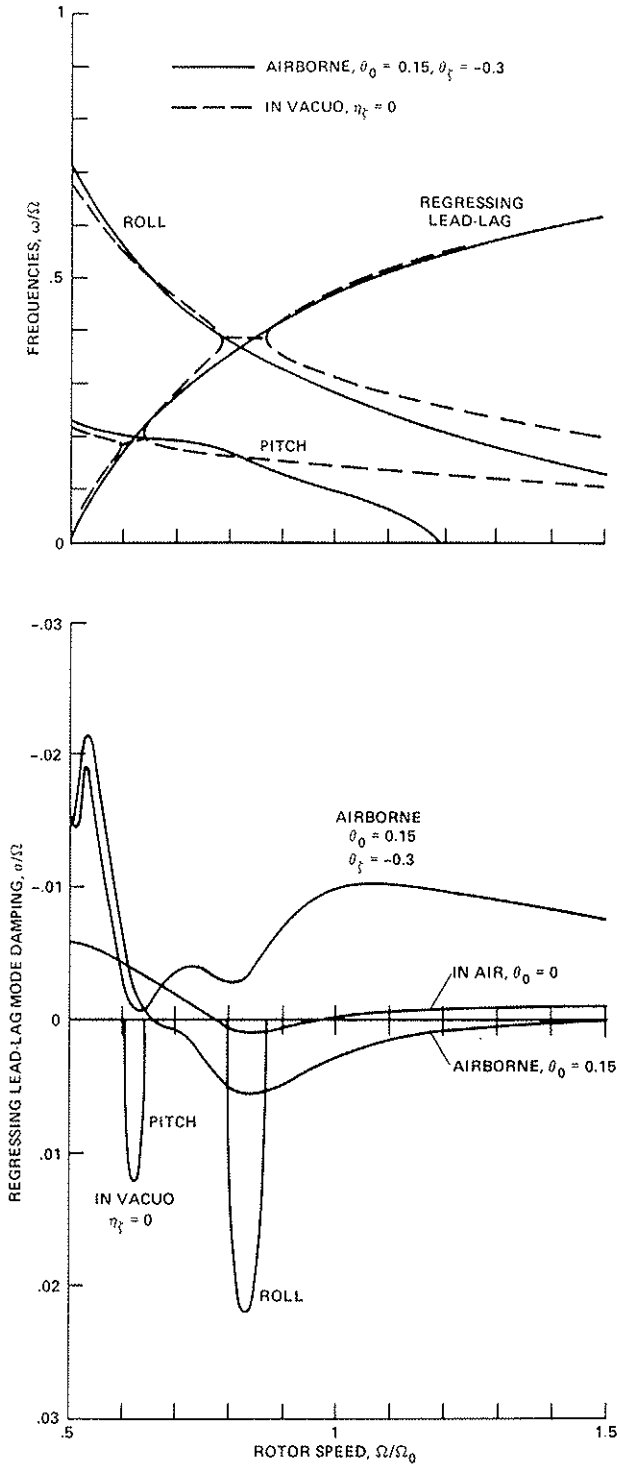

Fig. 24. Air resonance frequency and damping characteristics vs rotor speed at constant rotor thrust for a typical matched stiffness configuration, β, ζ, Θ, Φ, X, Y degrees of freedom, k_x = 0.2, k_y = 0.4, θ_o = 0.15, p_o = 1.118, $\bar{\omega}_{\zeta_o}$ = 0.5.

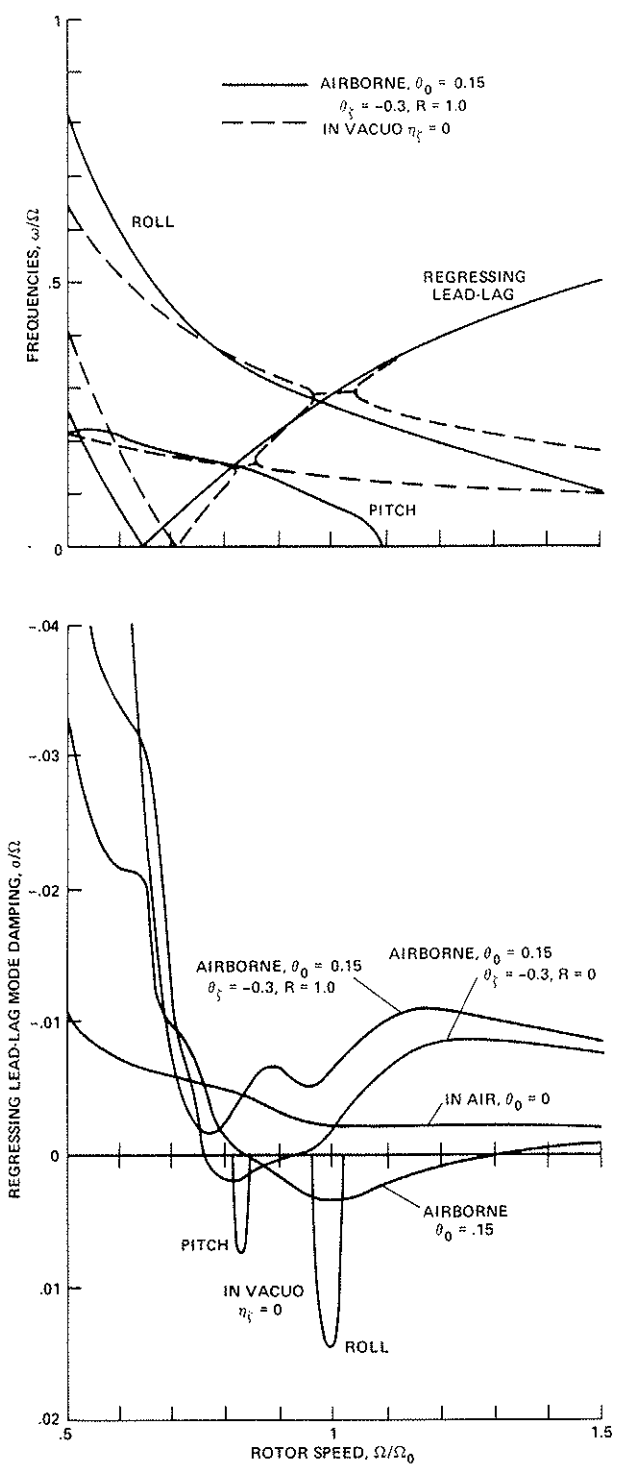

Fig. 25. Air resonance frequency and damping characteristics vs rotor speed at constant rotor thrust for a typical nonmatched stiffness configuration, β, ζ, Θ, Φ, X, Y degrees of freedom, k_x = 0.2, k_y = 0.4, Θ_o = 0.15, p_o = 1.1, $\bar{\omega}_{\zeta_o}$ = 0.5.

and thus the air resonance appears to become even more exclusively a roll-mode instability. It is not possible to add flap-lag structural coupling to the matched stiffness configuration but pitch-lag coupling can be added. As anticipated from previous results, pitch-lag coupling does stabilize the roll-mode instability but, surprisingly, it also destabilizes the pitch mode. Nevertheless, the system is now stable over the entire rotor speed range in Fig. 24 when pitch-lag coupling is included. A discussion is given in Ref. 11 of how pitch-lag coupling can be generated for matched-stiffness rotor blades.

The nonmatched stiffness configuration damping and frequency characteristics are shown in Fig. 25. The *in vacuo* pitch- and roll-mode instabilities are weaker than the matched stiffness result because the frequency resonance occurs "farther down" (lower p and higher $\bar{\omega}_\zeta$ values) on the resonance line in the p, $\bar{\omega}_\zeta$ plane where the mechanical instabilities are weaker. The instabilities occur closer to the nominal rotor speed than the matched stiffness configuration because the nominal regressing lead-lag mode frequency is nearly coincident with the roll-mode frequency. Again, the roll-mode instability is stronger than the pitch mode. With lead-lag structural damping and zero pitch angle aerodynamics, both the pitch- and roll-mode instabilities are eliminated. The damping versus rotor speed shows little evidence of the pitch mode and only a slight reduction in damping at the roll mode frequency coalescence. With the rotor in a thrusting condition, $\theta_0 = 0.15$, both the roll and pitch modes are destabilized and the roll mode becomes unstable over a moderately wide rotor speed range. With the introduction of aeroelastic couplings, the air resonance instability can be suppressed for this configuration. As in the case of the matched stiffness rotor, pitch-lag coupling is effective in stabilizing the roll mode but produces a pitch-mode instability. With the introduction of flap-lag structural coupling in addition to pitch-lag coupling, it is possible to eliminate both the roll- and pitch-mode instabilities. In this case, we set the structural coupling parameter $R = 1.0$ where $\theta_s = \theta$. Since θ increases with decreasing rotor speed to maintain constant rotor thrust, the flap-lag structural coupling increases with reduced rotor speed. The final configuration is seen to be stable over the entire rotor speed range.

10. Concluding Remarks

The intent of the research reported in this paper has been to develop a better understanding of some of the fundamental properties of hingeless rotorcraft air and ground resonance. Listed below are some of the major fundamental characteristics of these aeromechanical phenomena. Also included are the major effects of aeroelastic couplings on ground and air resonance stability.

1. Rotor flapping motion and flapping stiffness modify classical ground resonance by reducing the maximum value of $\bar{\omega}_\zeta$ at which mechanical instability can occur.

2. Along with the primary ground resonance instability, resonance of the regressing flap and regressing lead-lag modes produces a weak mechanical instability *in vacuo*. In the limit as the uncoupled body frequency approaches zero, these two modes interchange and the ground resonance instability essentially becomes an *in vacuo* version of air resonance.

3. The effects of structural damping on ground resonance *in vacuo* are strongly dependent on the ratio of blade lead-lag damping to body damping. When the blade and body damping are of the same order of magnitude, damping generally stabilizes the system. Unusual results may occur when the rotor and body damping are highly dissimilar. In extreme cases, mechanical instability can even occur for stiff inplane rotor configurations.

4. Like certain combinations of structural damping, aerodynamics in the absence of structural damping can be destabilizing. Increasing collective pitch is also generally destabilizing for ground resonance.

5. While the effects of flap damping of hingeless rotors are generally beneficial for ground resonance, increased flapping stiffness is not always beneficial. For high body frequencies (stiff landing gear), increasing p is generally stabilizing but for low body frequencies, increasing p is destabilizing. Increasing p is generally beneficial in that it lowers the maximum value of $\bar{\omega}_\zeta$ at which ground resonance can occur for any body frequency.

6. Air resonance is caused by resonance between the rotor regressing lead-lag mode and body pitch (or roll) mode. The body mode is a "free-free" mode arising mainly from the rotor-flap regressing mode and is controlled primarily by blade flap stiffness and body pitch (or roll) inertia. Increasing p and decreasing $\bar{\omega}_\zeta$ generally destabilizes air resonance.

7. Increasing body inertia strongly stabilizes air resonance. As a result, roll-mode air resonance tends to be much more serious than pitch-mode air resonance. Pitch-roll coupling does not appear to significantly influence air resonance.

8. Air resonance is generally worsened by increasing the rotor collective pitch.

9. The effects of aeroelastic couplings are generally not beneficial for ground resonance at zero collective pitch. At positive collective pitch, pitch-lag coupling and flap-lag structural coupling are effective in stabilizing ground resonance.

10. The combination of pitch-lag and flap-lag structural coupling is found to be very important in stabilizing air resonance. Without such aeroelastic couplings, increased lead-lag structural damping must be provided.

11. Matched stiffness configurations without aeroelastic couplings are found to be inherently more sensitive to air resonance instability than nonmatched stiffness configurations because of the larger p lower $\bar{\omega}_\zeta$ combination of blade frequencies.

REFERENCES

1. Coleman, Robert P. and Feingold, Arnold M., Theory of self-excited mechanical oscillations of helicopter rotors with hinged blades, NACA TR-1351, 1958.

2. Lytwyn, R. T., Miao, W., and Woitch, W., Airborne and ground resonance of hingeless rotors, Journal of the American Helicopter Society, Vol. 16, No. 2, April 1971.

3. Donham, R. E., Cardinale, S. V., and Sachs, I. B., Ground and air resonance characteristics of a soft inplane rigid rotor system, Journal of the American Helicopter Society, Vol. 14, No. 4, October 1969.

4. Baldock, J. C. A., Some calculations for air resonance of a helicopter with non-articulated rotor blades, RAE Technical Report 72083, August 1972.

5. Ormiston, Robert A., Concepts for improving hingeless rotor stability, paper presented at the American Helicopter Society Mideast Region Symposium on Rotor Technology, Essington, PA, August 1976.

6. Ormiston, Robert A. and Hodges, Dewey H., Linear flap-lag dynamics of hingeless helicopter rotor blades in hover, Journal of the American Helicopter Society, Vol. 17, No. 2, April 1972.

7. Ormiston, R. A. and Bousman, W. G., A study of stall-induced flap-lag instability of hingeless rotors, Journal of the American Helicopter Society, Vol. 20, No. 1, January 1975.

8. Hohenemser, K. H. and Yin, S. K., Some applications of the method of multiblade coordinates, Journal of the American Helicopter Society, Vol. 17, No. 3, July 1972.

9. Ormiston, Robert A., Equations of motion for a hingless rotor helicopter in hovering flight, NASA TM-73,270, in preparation.

10. Hodges, Dewey H. and Ormiston, Robert A., Stability of elastic bending and torsion of uniform cantilever rotor blades in hover with variable structural coupling, NASA TN D-8192, April 1976.

11. Hodges, Dewey H. and Ormiston, Robert A., Stability of hingeless rotor blades in hover with pitch link flexibility, AIAA Journal, Vol. 15, No. 4, April 1977.

NOTATION

a	blade airfoil section lift curve slope, rad^{-1} (2π)
b	number of blades
c	blade chord
h	distance from body center of mass to rotor hub, ft
$\bar{h}$	h/R
I	blade inertia about flap and lead-lag hinges, $\frac{1}{3} mR^2$, slug-ft^2
$I_{\Theta,\Phi}$	rotor and body pitch and roll inertia about body center of mass $I_\Theta = I_y + bI/2 + 3bI\bar{h}^2$, slug-$ft^2$
I_X, I_Y	body roll and pitch inertia about body center of mass, slug-ft^2
k_x, k_y	body mass radii of gyration in roll and pitch, $k_y = \sqrt{I_Y/m_f}$, ft
$\bar{k}_x, \bar{k}_y$	k_y/R
K_X, K_Y	effective landing gear spring constants for translation in X, Y directions, lb/ft
K_θ, K_ϕ	effective landing gear spring constants for pitch and roll rotations, ft-lb/rad
m	mass of one blade, slugs
m_f	mass of body, slugs
M	total mass of rotor-body, $m_f + bm$, slugs
p	dimensionless blade uncoupled flap frequency, $\sqrt{1 + \bar{\omega}_\beta^2}$
R	blade radius, ft
t	time, sec
X,Y,Z	body fixed coordinate system, origin at body center of mass
X_R, Y_R, Z_R	rotating rotor fixed coordinate system, origin at rotor hub

β	blade flap rotation about flap hinge, rad, positive up
β_c, β_s	cyclic multiblade coordinates for rotor flap deflections, rad
γ	blade Lock number, $\rho a c R^4/I$
ζ	blade lead-lag rotation about lead-lag hinge, rad, positive for lead
ζ_c, ζ_s	cyclic multiblade coordinates for rotor lead-lag deflections, rad
η_ζ, η_θ	structural damping ratio of blade lead-lag deflections and body pitch motions
θ	rotor blade collective pitch angle, rad
θ_s	inclination of principal axes of blade spring restraint system, Fig. 2, Eq. (1)
θ_{s_o}	value of θ_s when $\theta = 0$
θ_ζ	kinematic pitch-lag coupling parameter, positive if blade pitch angle increases when blade moves in direction of rotation (leads)
Θ	body pitch rotation about body X axis, rad
μ	rotor-body mass ratio, bm/M
ρ	air density, slugs/ft^3
σ	rotor solidity $\frac{bc}{\pi R}$, or real part of eigenvalue, sec
Φ	body roll rotation about Y axis, rad
ψ	rotor blade azimuth position, rad
ω	imaginary part of eigenvalue, rad/sec
ω_X, ω_Y	uncoupled body frequencies in translation $\omega_X = \sqrt{K_X/M}$, rad/sec
$\omega_\beta, \omega_\zeta$	uncoupled blade flap (nonrotating) and lead-lag frequencies $\sqrt{K_\beta/I}$, $\sqrt{K_\zeta/I}$, rad/sec
$\omega_\theta, \omega_\phi$	uncoupled body pitch and roll frequencies $\sqrt{K_\theta/I_\theta}$, $\sqrt{K_\phi/I_\phi}$, rad/sec
$\bar{\omega}_\Delta^2$	flap-lag structural coupling parameter, $\bar{\omega}_\zeta^2 - \bar{\omega}_\beta^2$
Ω	rotor angular velocity, $d\psi/dt$, rad/sec
$(\ )_o$	equilibrium deflection (i.e., β_o, ζ_o) or parameter defined at normal rotor speed (i.e., Ω_o, $\bar{\omega}_{\zeta_o}$, p_o)
$(\ )'$	$\frac{d(\ )}{d\psi}$, $\frac{1}{\Omega}\frac{d(\ )}{dt}$
$(\bar{\ })$	made dimensionless by rotor speed, i.e., $\bar{\omega}_\zeta = \omega_\zeta/\Omega$